ISSN 0036-0244, Russian Journal of Physical Chemistry A, 2014, Vol. 88, No. 12, pp. 2165–2171. © Pleiades Publishing, Ltd., 2014.
Original Russian Text © S.V. Shevkunov, 2014, published in Zhurnal Fizicheskoi Khimii, 2014, Vol. 88, No. 12, pp. 1963–1969.

PHYSICAL CHEMISTRY
OF NANOCLUSTERS AND NANOMATERIALS

Thermodynamic Characteristics of the Hydrate Shell of a Na^+ Ion in a Plane Nanopore with Hydrophobic Walls

S. V. Shevkunov

St. Petersburg State Polytechnic University, St. Petersburg, 195251 Russia

e-mail: shevk54@mail.ru

Received February 15, 2013

Abstract—The chemical potential, free energy, and work of hydration of a single-charged sodium cation are calculated using the Monte Carlo method for a bicanonic statistic ensemble at the molecular level at 298 K in plane model nanopores 0.5 and 0.7 nm wide. It is shown that the nanopores have a stabilizing effect on the hydrate shell of an ion. It is concluded that the crisis of stability that occurs outside a pore is transformed into an abrupt acceleration of growth with the conservation of a stable equilibrium with vapor under the conditions of plane nanopores. It is established that the mechanism of the threshold acceleration of growth inside a pore is associated with an ion being displaced from its own hydrate shell.

Keywords: ion, hydration, nanopore, Monte Carlo method, free energy, entropy

DOI: 10.1134/S0036024414120309

INTRODUCTION

Despite the wide use of computer modeling to study the equilibrium properties of molecular associates under conditions of thermal fluctuation [1–14], where calculations of free energy and entropy at the molecular level are difficult. These are calculated comparatively rarely [15] and are, as a rule, based on different indirect [16] or approximate schemes [17, 18], while the thermodynamics of growth from vapor in nanodimensional cavities has not been investigated with these methods at all [19]. In this work, we present the results from calculating the free energy, entropy, and work of hydration, along with the adsorption curves obtained via computer modeling of the same system as in our earlier study. We focus on the effect limited nanopore space has on the thermodynamic stability of hydration.

COMPUTATIONAL PROCEDURE

The chemical potential of molecules of a hydrate shell $\mu_{cl}(N, T)$ was calculated using a bicanonic statistic ensemble (BSA) [20–31]. The BSA method is a variety of the Monte Carlo method and is categorized as a reference method of numerical modeling at a molecular level. The statistical part of the problem is solved by this method, which considers all intermolecular correlations without using continuous media or average field approximations.

The detailed ICP(SPC) model was used to describe intermolecular interactions [32–40]. The model includes the Coulomb, exchange, and dispersion interactions, along with unpaired polarization interactions, unpaired covalent-type interactions, excess charge transfer, and screening effects. Corrections for the quantum character of molecular motion are considered in implicit form in the numerical values of parameters, restored from the fitting condition with the experimental data on the free energy and enthalpy of the first reactions of molecular attachment to the hydrate shells of free ions [41].

The equilibrium averages at room temperature $T =$ 298 K were calculated for water molecules in the field of a single-charged sodium cation fixed between structureless parallel plane pore walls 0.5 and 0.7 nm wide. Equilibrium characteristics were calculated by averaging over 10^8 molecular configurations. The frequency of new configuration acceptance varied from 30 to 50% at a maximum translational displacement of the molecule of 0.03 nm and a maximum angle of revolution of 20°. When computing the chemical potential [32–40], 10^9 attempts to vary the number of molecules in a system with a frequency of acceptance of ~0.2% were made for each thermodynamic state.

The Gibbs energy of N molecules was obtained via numerical summation of the computed values of chemical potential:

$$G_{cl}(N,T) = \sum_{n=1}^{n=N} \mu_{cl}(n,T) \text{ [42].}$$

The potential part of the internal energy of a hydrate shell in an ion field $U_{cl}(N,T)$ was computed separately via canonic averaging. The total energy in a model of rigid rotators in a system with an immobile ion was $E_{cl}(N,T) = U_{cl}(N,T) + (6N/2)k_BT$ and the enthalpy was $H_{cl}(N,p,T) = E_{cl}(N,T) + pV_{cl}$ [42], where V_{cl} is the volume occupied by a hydrate shell. Shell entropy

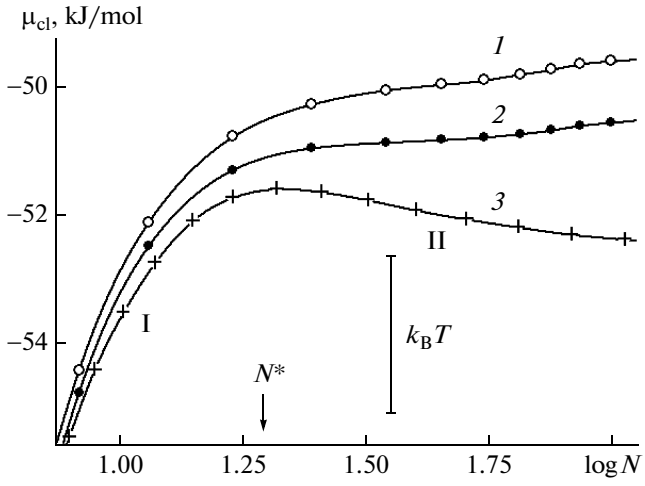

Fig. 1. Chemical potential of the molecules of an Na^+ ion hydrate shell at 298 K in the size area corresponding to the hydration mode changing from enveloping to asymmetric (*1*) in a plane pore 0.5 nm wide, (*2*) in a plane pore 0.7 nm wide, and (*3*) outside a pore. For other notations, see the text.

$S_{cl} = (H_{cl} - G_{cl})/T$. The entropy of vapor molecule attachment to the hydrate shell was calculated as $\Delta S(N, p, T) = (\Delta H(N,T) - \Delta G(N, p,T))/T$. Under the conditions of a rarefied vapor $pV_{cl} \ll k_BT$, enthalpy of attachment $\Delta H(N, T) = U_{cl}(N,T) - U_{cl}(N-1,T) - pv_g = \Delta U_{cl}(N,T) - k_BT$, where $v_g = k_BT/p$ is the volume per one vapor molecule, $\Delta U_{cl}(N, T) = U_{cl}(N,T) - U_{cl}(N-1,T)$ is the variation in the potential part of the internal energy of the hydrate shell due to the attachment of one molecule, and Gibbs energy of attachment $\Delta G(N, p, T) = \mu_{cl}(N, T) - \mu(p, T)$. Vapor pressure p was an input parameter for computations. A model of an ideal gas of rigid rotators was used to recalculate the pressure to the corresponding chemical potential of vapor molecules $\mu(p,T)$ and vice versa [43]:

$$\mu(p,T) = -k_BT \ln\left(\frac{8\pi^2}{\sigma}\frac{k_BT}{p} Z_{tr}^{kin} Z_{rot}^{kin}\right), \qquad (1)$$

where $Z_{tr}^{kin} = \left(\frac{h}{(2\pi m k_BT)^{1/2}}\right)^{-3} = \frac{1}{\Lambda^3}$ is the result from integration by moments of translatory motion, while $Z_{rot}^{kin} = \frac{(2k_BT)^{3/2}(I_1I_2I_3)^{1/2}\pi^{3/2}}{h^3}$ for the angular impulses of water molecules in a statistical sum; I_1, I_2, and I_3 are the principal moments of inertia; m is the molecular mass; h is the Plank constant; Λ is the thermal length of a de Broglie wave; and σ is the rotational symmetry parameter for molecules (=2 for water).

Results for the entropy of attachment were in calculating to standard vapor pressure $p_0 = 1$ atm. Reduction to pressure p_0 was accomplished using the formula $\Delta S(n, p_0, T) = \Delta S(n, p, T) + k_B\ln(p_0/p)$, from which we can see that the entropy of the attachment curve shifts as a whole without changing its shape upon variations in pressure.

THERMODYNAMIC CHARACTERISTICS

Chemical Potential

The chemical potential of the molecules of a hydrate shell μ_{cl} inside and outside a nanopore behaves differently (Fig. 1). Under the conditions of the limited space of a plane nanopore, μ_{cl} rises monotonically with the accumulation of molecules (curves *1*, *2*), while outside a nanopore (curve *3*) it first rises (branch I) and then falls after passing its maximum near $N^* \approx 20$ (branch II). The increase in the chemical potential at low N is due mainly to an increase in the energy of direct interactions with the ion due to the greater average distance between the ion and the molecules. As the hydrate shell shrinks, the relative fraction of direct interactions with the ion diminishes and the fraction of interactions with other molecules grows. The energy of interactions with other molecules falls because of an increase in the average number of nearest neighbors. After reaching threshold number of molecules N^*, the drop in the energy of molecule–molecule interactions prevails over the increased energy of molecule–ion interactions, and the increase in the Gibbs energy of attachment and the chemical potential is replaced by their reduction.

Variations in entropy component $-TS$ are superimposed on these changes in binding energy; allowing for the negative sign with which they enter the free energy, they run opposite to the variations in energy, but are somewhat smaller than the latter in absolute magnitude. The variations in entropy only smooth the rise and drop in energy without fully compensating for them in the chemical potential. The formation of the maximum in the dependence of the chemical potential of the hydrate shell of a free ion in Fig. 1 must thus be interpreted as an energy effect. The energy effects grow with a drop in temperature.

From the viewpoint of a capillary approximation, a drop in the chemical potential upon the growth of a microdrop is interpreted as a reduction in the relative fraction of positive surface contributions in the free energy of the system, relative to negative bulk contibutions. This drop is inevitable in homogenous (ion-free) compact microdrops. The transition from rising to falling chemical potential can be considered a sign of the transition to the homogeneous growth mode.

Thermodynamic Stability

It is well known that the homogeneous nuclei of a condensed phase are thermodynamically unstable in the gas phase; when they exceed critical size N_s, they transition to the avalanche growth mode. The reason

for this thermodynamic instability is the chemical potential falling with size. The negative sign of the first derivative of the chemical potential indicates the concave shape of the Gibbs energy dependence $\frac{\partial \mu_{cl}(N,T)}{\partial N} = \frac{\partial^2 G_{cl}(N,p,T)}{\partial N^2} < 0$, which in turn, at values of pressure p that allow material equilibrium between vapor and a drop, yields the curve of the work of formation

$$A(N,p,T) = G_{cl}(N,T) - N\mu(p,T) \quad (2)$$

and ensures that there will be a maximum at equilibrium point $\mu_{cl}(N_s,T) = \mu(p,T)$:

$$\frac{\partial A(N,p,T)|}{\partial N}|_{N=N_s} = 0;$$

$$\frac{\partial^2 A(N,p,T)|}{\partial N^2}|_{N=N_s} = \frac{\partial^2 G_{cl}(N,T)|}{\partial N^2}|_{N=N_s} < 0.$$

The location of this maximum corresponds to critical nucleus size N_s [44], and its overcoming of fluctuation is accompanied by a loss of equilibrium and the avalanche growth of the microdrop. In contrast, the growing dependence of the chemical potential on size results in the positive value of the second derivative

$$\frac{\partial^2 G_{cl}(N,p,T)}{\partial N^2} > 0,$$

the minimum in $A(N,p,T)$, and a stable equilibrium with the vapor.

It can be seen from the character of dependences in Fig. 1 that if the hydrate shell of the Na^+ ion in conditions outside a pore is stable at $N < N^*$ and unstable at $N > N^*$, the hydrate shell of the ion is always stable under the conditions of a plane nanopore. The nanopore has a stabilizing effect on the hydrate shell.

The stability of the Na^+ ion's hydrate shell was the subject of special investigation in [45]. The point of the crisis of stability $N = N^*$ is the inflection point in the dependence of the Gibbs energy on its size. Its position depends on the temperature but is independent of the vapor pressure. The analysis in [45] showed that stability is lost at the same time the ion is displaced from its own hydrate shell, and a cluster of water molecules with the ion on its surface is formed. In this configuration, the hydrate shell (which envelops the ion from all sides) is transformed into a hydrate cluster that resembles a homogeneous drop with an ion on its surface. It is natural to attribute the loss of system stability due to such transformations to the instability characteristic of homogeneous microdrops.

We might assume that the ion's displacement from its hydrate shell (see our earlier article about system structure) under nanopore conditions would also be accompanied by a loss of stability. However, the trend of curves *1* and *2* in Fig. 1 does not confirm this assumption. The ion is displaced from the hydrate shells in plane nanopores, but this phenomenon is not accompanied by a loss of thermodynamic stability. The physical reason for the enhanced stability lies in the plane shape of the cluster that it accepts in a nanopore. The role of surface contributions to a plane microdrop is played by the excess free energy at the edges. The number of molecules at the edges of a plane microdrop is lower than the number of surface molecules in a bulk microdrop of the same size N. Therefore, the free energy's deviation from linearity with respect to N (the reason for the convex shape of the work of formation curve) is also smaller for a plane microdrop.

Crisis of Stability

The boundary between stable and unstable states can be also clearly observed in the dependences of the work of hydration in Fig. 2a. Concave curves *1* and *2* (which correspond to nanopore conditions) remain concave at any N, while curve *3* (which corresponds to hydration conditions outside a pore) has an inflection point at $N = N^*$, where it transitions from a concave to a convex shape. To extend the curve into the region of the unstable state ($>N$), we were forced to use the logarithmic scale in Fig. 2b. Generally speaking, the presence of the inflection point in the logarithmic scale does not mean that it also exists in the linear scale, but the existence of extrema is independent of the applied scale, and the simultaneous existence of a minimum and the maximum inevitably results in an inflection point between them.

The dependences of the work of hydration in Fig. 2b are presented for the pressure at which the minimum and the maximum exist simultaneously in curve *3*, and there is an inflection point between them in the linear scale. The location of this point $N = N^*$ between the stable (branch I) and unstable (branch II) states corresponds to a crisis of stability and is independent of the vapor pressure. The crisis of stability of a hydrate shell is observed under the conditions outside a pore and not in plane nanopores, where the hydrate shell of the sodium cation maintains the equilibrium stability with vapor over the range of sizes.

Avalanche evaporation in systems with a crisis of stability does not end with the complete disappearance of the molecular associate. Local minimum $A(N,p,T)$ found in region $N < N^*$ and stabilizing the system prevents subsequent evaporation (curve *3* in Fig. 2b). Complete evaporation is unfavorable thermodynamically if $A(N,p,T)$ in the maximum has a negative value, as in the case of curve *3* in Fig. 2b.

Extremum of the Work of Hydration

The work of formation of a microdrop (hydrate shell) from vapor in thermal and material equilibrium with it is an effective indicator of thermodynamic stability. The expression for the work of formation at extreme point $A(N,p,T)$

$$A^{eq}(N,T) = G_{cl}(N,T) - N\mu_{cl}(N,T) \quad (3)$$

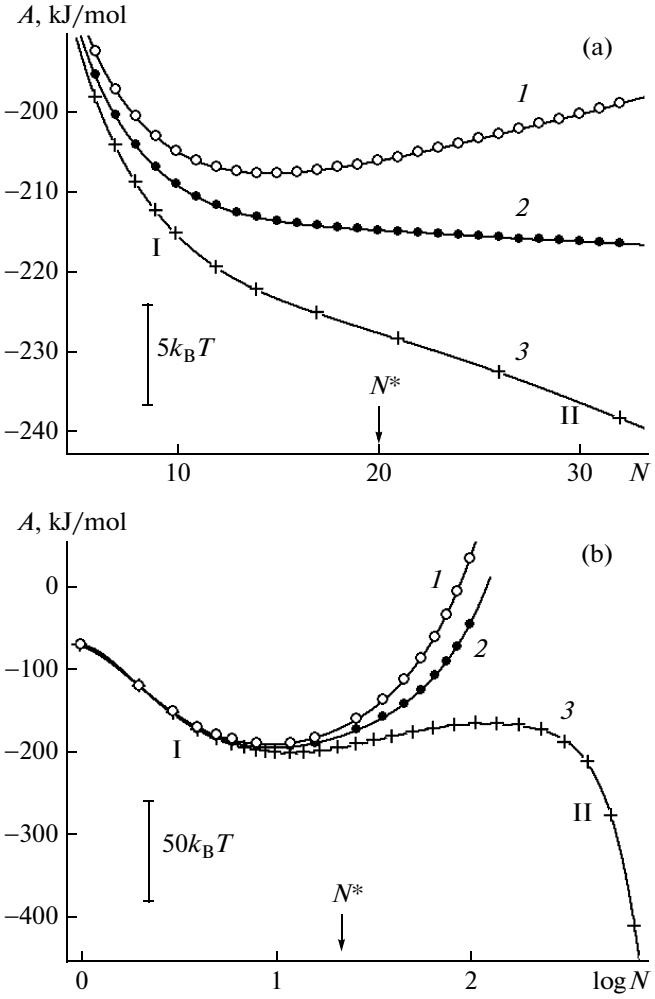

Fig. 2. Work of equilibrium hydration of an Na^+ ion at 298 K in water vapor at pressures of (a) 16.8 and (b) 8.4 kPa as a function of hydrate shell size: (*1*) in a plane pore 0.5 nm wide, (*2*) in a plane pore 0.7 nm wide, and (*3*) outside a pore. For other notations, see the text.

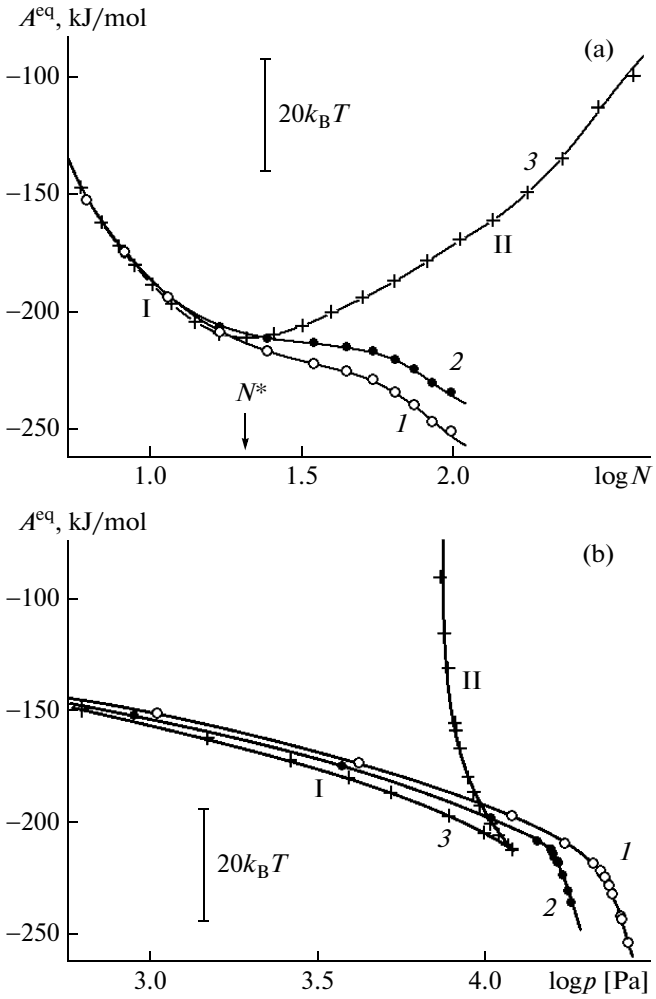

Fig. 3. Work of hydration of an Na^+ ion at 298 K in saturated water vapor, relative to a hydrate shell with size N as a function of (a) size and (b) vapor pressure: (*1*) in a plane pore 0.5 nm wide, (*2*) in a plane pore 0.7 nm wide, and (*3*) outside a pore. For other notations, see the text.

follows from (2), allowing for the material equilibrium condition between the microdrop and vapor $\mu(p, T) = \mu_{cl}(n, T)$. $A^{eq}(N,T)$ is the magnitude of work $A(N, p,T)$ at its extreme point $N = N_s(p)$. If there is one extreme, positivity $A^{eq}(N,T) > 0$ at an extreme point (allowing for $A(0, p,T) = 0$) means that it is a maximum; curve $A(N, p,T)$ is thus convex, indicating instability. In contrast, negativity $A^{eq}(N,T) < 0$ indicates curve $A(N, p,T)$ is concave, meaning the system is stable. As demonstrated by curves *1* and *2* in Fig. 3a, negative values of $A^{eq}(N,T)$, measured in tens of k_BT, yield an estimate of the degree of stability of a hydrate shell under nanopore conditions.

The case is more complex if $G_{cl}(N,T)$ has an inflection point; its second derivative changes sign, and $A(N, p,T)$ can have several extrema. The sign of $A^{eq}(N,T)$ is no longer clearly associated with the shape of the Gibbs energy curve, but its concavity or convexity can be judged by the direction of the change in $A^{eq}(N,T)$. According to (3),

$$\frac{\partial A^{eq}(N,T)}{\partial N} = \frac{\partial G_{cl}(N,T)}{\partial N} - \mu_{cl}(N,T) - N\frac{\partial \mu_{cl}(N,T)}{\partial N} \quad (4)$$

or allowing for identities $\frac{\partial G_{cl}(N,T)}{\partial N} = \mu_{cl}(N,T)$ and $\frac{\partial^2 G_{cl}(N,T)}{\partial N^2} = \frac{\partial \mu_{cl}(N,T)}{\partial N}$,

$$\frac{\partial^2 G_{cl}(N,T)}{\partial N^2} = -\frac{1}{N}\frac{\partial A^{eq}(N,T)}{\partial N}. \quad (5)$$

In particular, it follows from (5) that

$$\frac{\partial A^{eq}(N,T)}{\partial N} = -N\frac{\partial \mu_{cl}(N,T)}{\partial N}.$$

Extreme $A^{eq}(N,T)$ now lies at the same point $N = N^*$ as extreme $\mu_{cl}(N,T)$, and we have a minimum instead of a maximum.

We can see in Fig. 3a that curve *3* has a minimum at point $N = N^*$ that separates the descending (branch I) from the ascending (branch II). According to (5), $\frac{\partial^2 G_{cl}(N,T)}{\partial N^2} > 0$ for the first branch, and the hydrate shell is in stable equilibrium with the vapor; in the second branch, the equilibrium is unstable.

Pressure Dependences

A contrasting pattern of division into two branches can be seen in the dependences for vapor over a pore. The direction of change for $A^{eq}(N_s(p),T)$ upon variations in pressure depends on the direction of the change in equilibrium size $N_s(p)$:

$$\frac{\partial A^{eq}(N_s(p),T)}{\partial p} = \frac{\partial A^{eq}(N,T)}{\partial N}\Big|_{N=N_s(p)} \frac{\partial N_s(p)}{\partial p}. \quad (6)$$

On the other hand, the direction of change for $N_s(p)$ is clearly associated with the convexity or concavity of $G_{cl}(N,T)$ (i.e., the stability of the system). In the equilibrium state between a nucleus and vapor, it follows from equalities $\frac{\partial^2 G_{cl}(N,T)}{\partial N^2}\Big|_{N=N_s} = \frac{\partial \mu(p,T)}{\partial p}\left(\frac{\partial N_s(p)}{\partial p}\right)^{-1}$ and (1) that

$$\frac{\partial N_s(p)}{\partial p} = \frac{k_B T}{p}\left(\frac{\partial^2 G_{cl}(N,T)}{\partial N^2}\Big|_{N=N_s}\right)^{-1}. \quad (7)$$

With unstable states, the left part of (7) is negative, and function $A^{eq}(N, T)$, ascending with N, is the descending function of pressure p, according to (6). In this orientation, branch II of curve *3* in Fig. 3b lies above branch I. The violation of the clarity of function reflects the presence of two extrema in curve *3* in Fig. 2b that correspond to two equilibrium sizes, one of which is stable (branch I), while the second is unstable (branch II). These features are characteristic of a crisis of stability, are reproduced during the hydration of a free ion, and are not seen under the conditions of plane nanopores: curves *1* and *2* in Fig. 3b are not divided into two branches, as in the case of curve *3*.

Entropy

The entropy of the attachment reaction at $N = 4$ shows a sharp minimum that is also retained upon hydration in nanopores in Fig. 4. An abrupt drop in entropy reflects the formation of a relatively rigid construction. Analysis of molecular configurations shows that the first four molecules attach themselves immediately to a sodium ion, while subsequent molecules attach themselves to the first four and thus start to form chains that radiate from the ion.

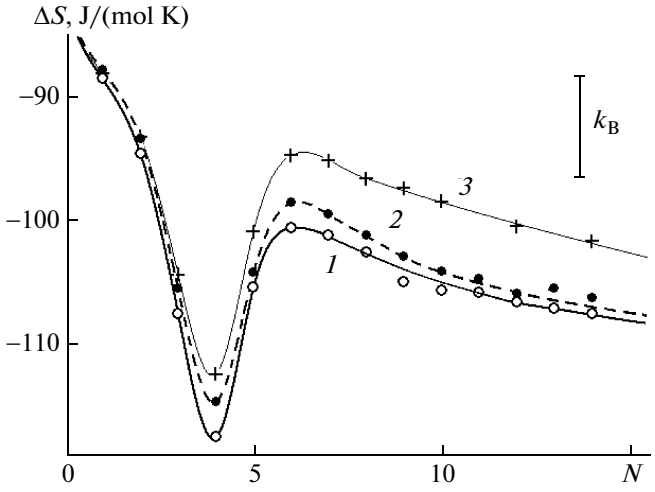

Fig. 4. Entropy of vapor molecule attachment to an Na^+ ion hydrate shell, reduced to the standard vapor pressure of 1 atm at 298 K in small-size region N: (*1*) in a plane pore 0.5 nm wide, (*2*) in a plane pore 0.7 nm wide, and (*3*) outside a pore.

Two branches corresponding to stable (I) and unstable (II) states form in the pressure dependences of specific entropy in the size of regions corresponding to ion displacement from hydrate shells under the conditions outside a pore (Fig. 5, curve *3*). No division into two branches is seen under nanopore conditions (curves *1* and *2*), while the descending trend of the curves corresponds to monotonic growth and the densification of hydrate clusters.

Adsorption Curves

The dependence of the equilibrium size on the vapor pressure in the same size region for pore conditions (Fig. 6, curves *1* and *2*) ascends monotonically; while it splits into two branches outside a pore (curve *3*), ascending (I) and descending (II) notably. According to (6), ascending dependence $N_s(p)$ in the limits of branch I indicates the positive sign of the second derivative of the Gibbs energy and testifies to the thermodynamic stability of the system. The descending curve in the limits of branch II indicates instability. The monotonic rise of curves *1* and *2* confirms the thermodynamic stability of hydration under nanopore conditions over the range of sizes.

The shape of the adsorption curves in Fig. 6 indicates the threshold character of the penetration of molecules into pores with ions. The hydrate shell of an ion in saturated water vapor (the vapor pressure at 298 K is ≈3 kPa) both in and out of a pore consists of seven–eight molecules. An rise in vapor pressure up to fivefold supersaturation is accompanied by relatively slow growth of the hydrate shell to $N^* \approx 20$ molecules,

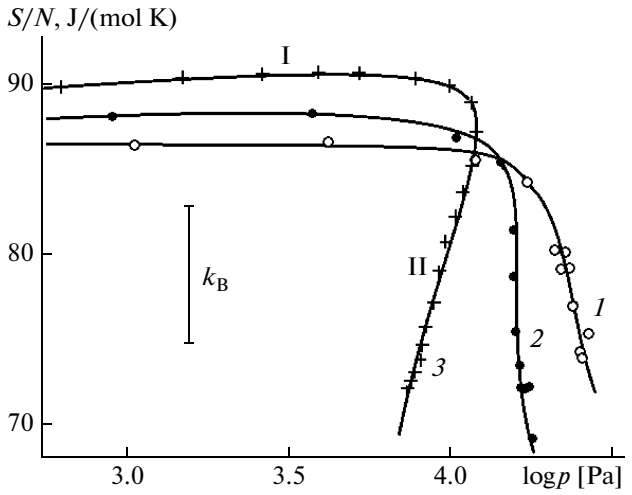

Fig. 5. Specific entropy of an Na^+ ion hydrate shell at 298 K as a function of saturating vapor pressure relative to a hydrate shell of corresponding size *N:* (*1*) in a plane pore 0.5 nm wide, (*2*) in a plane pore 0.7 nm wide, and (*3*) outside a pore. For other notations, see the text.

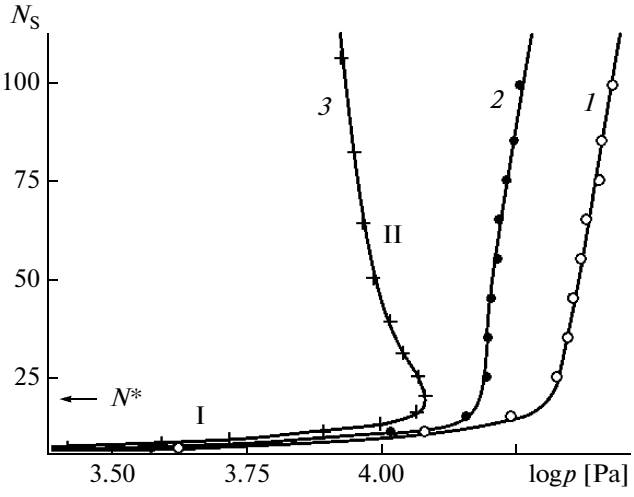

Fig. 6. Equilibrium size of a Na^+ ion hydrate shell at 298 K as a function of saturated vapor pressure relative to size in the region corresponding to the transition from the enveloped to the asymmetric hydrate mode: (*1*) in a plane pore 0.5 nm wide, (*2*) in a plane pore 0.7 nm wide, and (*3*) out of the pore. For other notations, see the text.

after which the growth inside the pore accelerates abruptly but does not exit from the equilibrium mode. Outside a pore, it is transformed into avalanche condensation.

CONCLUSIONS

Mechanical contact does not ensure the penetration of liquid water into a plane nanopore with hydrophobic walls; however, water can be present in the nanopores in the hydrate shells of ions. Each single-charge sodium cation holds approximately eight water molecules at room temperature and saturated water vapor covers each pore. Further growth of the ion hydrate shell is possible only in supersaturated pores.

At the same time, a hydrate ion shell remains stable outside a pore only to a size of approximately of 20 molecules, after which avalanche condensation develops. In plane nanopores, hydration continues in the equilibrium mode until a pore is filled completely. Only abrupt acceleration of equilibrium shell growth is observed in the size region corresponding to the crisis of stability outside a pore.

An approximately fivefold excess of the partial pressure over a pore relative to the saturation pressure is needed to fill a pore with water completely.

ACKNOWLEDGMENTS

This work was supported by the RF Ministry of Education and Science; and by the Russian Foundation for Basic Research, project no. 13-03-00062_a.

REFERENCES

1. A. V. Mokshin and D. N. Galimzyanov, J. Phys. Chem. B **116**, 11959 (2012).
2. J. Yin and D. P. Landau, J. Chem. Phys. **134**, 074501 (2011).
3. A. Y. Galashev, Mol. Simul. **36**, 273 (2010).
4. J. Gelman-Constantin, M. A. Carignano, I. Szleifer, et al., J. Chem. Phys. **133**, 024506 (2010).
5. D. Kang, J. Dai, Y. Hou, and J. Yuan, J. Chem. Phys. **133**, 014302 (2010).
6. Y. Zhang, H. S. Chen, B. X. Liu, et al., J. Chem. Phys. **132**, 194304 (2010).
7. R. D'Auria, I.-F. W. Kuo, and D. J. Tobias, J. Phys. Chem. A **112**, 4644 (2008).
8. G.-J. Guo, Y.-G. Zhang, M. Li, and Ch.-H. Wu, J. Chem. Phys. **128**, 194504 (2008).
9. L. Cwiklik, U. Buck, W. Kulig, et al., J. Chem. Phys. **128**, 154306 (2008).
10. M. Salonen, I. Napari, and H. Vehkamaki, Mol. Simul. **33**, 245 (2007).
11. M. Galvagno, D. Laria, and J. Rodriguez, J. Mol. Liq. **136**, 317 (2007).
12. S. F. Langley and E. Curotto, J. Chem. Phys. **126**, 084506 (2007).
13. C. Caleman and D. van der Spoela, J. Chem. Phys. **125**, 154508 (2006).
14. C. J. Burnham, M. K. Petersen, T. J. F. Day, et al., J. Chem. Phys. **124**, 024327 (2006).
15. S. Merchant, P. D. Dixit, K. R. Dean, and D. Asthagiri, J. Chem. Phys. **135**, 054505 (2011).
16. M. Gruziel, W. R. Rudnicki, and B. Lesyng, J. Chem. Phys. **128**, 064503 (2008).
17. H. Matsubara, T. Koishi, T. Ebisuzaki, and L. Inci, J. Chem. Phys. **127**, 214507 (2007).
18. R. K. Bowles, J. Chem. Phys. **134**, 114505 (2011).

19. N. A. Lvova and O. Yu. Ananina, Russ. J. Phys. Chem. A **87**, 1515 (2013).
20. S. V. Shevkunov, Kolloidn. Zh. **45**, 1019 (1983).
21. S. V. Shevkunov, A. A. Martsinovski, and P. N. Vorontsov-Velyaminov, Teplofiz. Vys. Temp. **26**, 246 (1988).
22. S. V. Shevkunov, A. A. Martsinovski, and P. N. Vorontsov-Velyaminov, Mol. Simul. **5**, 119 (1990).
23. S. V. Shevkunov, Russ. J. Phys. Chem. A **76**, 499 (2002).
24. S. V. Shevkunov, Russ. J. Phys. Chem. A **78**, 1590 (2004).
25. S. V. Shevkunov, Russ. J. Gen. Chem. **74**, 1471 (2004).
26. S. V. Shevkunov, S. I. Lukyanov, J.-M. Leyssale, and Cl. Millot, Chem. Phys. **310**, 97 (2005).
27. S. I. Lukyanov, Z. S. Zidi, and S. V. Shevkunov, Chem. Phys. **332**, 188 (2007).
28. S. I. Lukyanov, Z. S. Zidi, and S. V. Shevkunov, J. Mol. Struct.: THEOCHEM **725**, 191 (2005).
29. S. I. Lukyanov, Z. S. Zidi, and S. V. Shevkunov, Fluid Phase Equilib. **233**, 34 (2005).
30. S. V. Shevkunov, Colloid. J. **67**, 497 (2005).
31. S. V. Shevkunov, Colloid. J. **68**, 632 (2006).
32. S. V. Shevkunov, Dokl. Phys. Chem. **356**, 341 (1997).
33. S. V. Shevkunov, Russ. J. Electrochem. **38**, 300 (2002).
34. S. V. Shevkunov, Russ. J. Phys. Chem. A **78**, 383 (2004).
35. S. V. Shevkunov, Colloid. J. **66**, 495 (2004).
36. S. V. Shevkunov, Colloid. J. **66**, 216 (2004).
37. S. V. Shevkunov, Colloid. J. **72**, 93 (2010).
38. S. V. Shevkunov, Russ. J. Electrochem. **49**, 228 (2013).
39. S. V. Shevkunov, Colloid. J. **68**, 632 (2006).
40. S. V. Shevkunov, J. Exp. Theor. Phys. **108**, 447 (2009).
41. M. Arshadi, R. Yamdagni, and P. Kebarle, J. Phys. Chem. **74**, 1466 (1970).
42. T. L. Hill, *Statistical Mechanics. Principles and Selected Applications* (McGraw-Hill, New York, 1956).
43. C. Kittel, *Thermal Physics* (Wiley, New York, 1969).
44. F. F. Abraham, *Homogeneous Nucleation Theory* (Academic Press, New York, London, 1974).
45. S. V. Shevkunov, Colloid. J. **73**, 275 (2011).

Translated by N. Korovin